PHYSICAL REVIEW A VOLUME 51, NUMBER 1 JANUARY 1995

# Multiple-charged secondary-ion emission from silicon and silicon oxide bombarded by heavy ions at energies of 0.4–10 MeV

S. Kyoh, K. Takakuwa, M. Sakura, M. Umezawa, A. Itoh, and N. Imanishi
*Department of Nuclear Engineering, Kyoto University, Yoshida-Honmachi, Sakyo-ku, Kyoto 606-01, Japan*
(Received 9 May 1994; revised manuscript received 25 July 1994)

Secondary-ion yields have been measured for Si and $SiO_2$ targets bombarded by C, Si, Ge, and Ag projectiles over an energy range between 0.4 and 10 MeV, where the atomic-collision process changes from a nuclear to an electronic one. Obtained yields of secondary $Si^{q+}$ ($q = 1, 2, 3, 4$) ions for the C projectiles are generally decreasing functions of incident energy. On the other hand, the yields for Ag increase with increasing energy except for $Si^+$. The possibility of multiple-charged recoil-ion production through the simultaneous process of ionization and recoil caused by the projectiles is discussed on the basis of an independent-electron model, which describes multiple ionization of atoms by energetic heavy-ion impact.

PACS number(s): 79.20.Nc

## I. INTRODUCTION

Secondary-ion emission is one of the most interesting and applicable phenomena in ion-solid interactions (see [1] and references cited therein). In the past decade great progress has been made on sputtering in a low-incident-energy region where the nuclear collision dominates over the electronic collision. The electron-tunneling model is very useful for explaining many general trends in secondary-ion emission from metals and semiconductors [2,3]. For ionic and partially ionic solids, the bond-breaking model is the most widely accepted mechanism to explain the large secondary-ion emission yields [4,5].

At high incident energies, however, phenomena that cannot be explained by the above mechanisms have been found. The first such results are unusually large yields of singly charged positive ions with high electronegativities [6–8]. Yields of multiple-charged positive metallic ions also increase with increasing beam energy [9–11]. A so-called kinetic model was then applied [12]. In this model, inner-shell holes are produced by the energetic collisions between target atoms ($TT$) and the presence of those holes is the major cause for the ionization of sputtered atoms at the high incident energies. The most widely accepted mechanism for the production of the inner-shell excitation is the electron-promotion model [13] because the energy required for the electron promotion is particularly small in symmetric $TT$ collisions in which the energy levels of the collision partners match each other [14]. The proposed ionization mechanisms of the sputtered atoms are based on the cascade process caused by the nuclear collisions.

However, Blauner and Weller found that the yield of $O^+$ emitted from metal oxide is wholly unrelated to the nuclear energy deposition [11,15]. In addition, sputtering yields of large organic molecules and frozen gases induced by MeV ion impact are correlated with the electronic energy deposition [16] and molecular dynamics in the field of electronic sputtering has been successfully applied [17].

So far, systematic experimental studies on the yields of multiple-charged secondary ions are limited below several hundred keV, where the nuclear-collision process dominates over the electronic process for heavy projectiles [18]. In the present study, therefore, we have extended the measurements to an energy range of MeV. In this energy range, even heavy ions have the electronic stopping powers $S_e$ higher than the nuclear ones $S_n$ [18], as shown in Fig. 1. Thus electronic collision may reveal a prominent role for the production of multiple-charged secondary ion in the present energy range where the nuclear energy deposition contributes only slightly. Solid targets of semiconductor-grade silicon and silicon oxide were used. Impact energies of 0.4–10 MeV of C, Si, Ge, and Ag species range from the competitive region of nuclear and electronic collisions to the dominant region of the electronic collision.

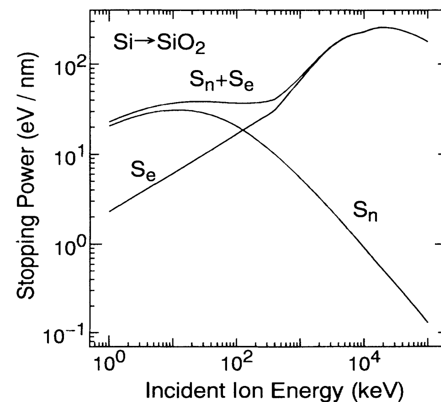


FIG. 1. Nuclear and electronic stopping powers $S_n$ and $S_e$ are plotted over a wide incident energy range for the projectile-target system of $Si$-$SiO_2$ [18].

1050-2947/95/51(1)/554(7)/$06.00  ©1995 The American Physical Society

## II. EXPERIMENT

Figure 2 shows the experimental arrangement. An ion beam from the Kyoto University 1.7-MeV tandem Cockcroft-Walton accelerator was collimated to a spot of 1 mm in diameter and incident on the Si or $SiO_2$ target at an angle of 70° with respect to the surface normal. The 400-nm-thick $SiO_2$ target was a sample fabricated by epitaxial growth on a silicon wafer. The resulting secondary atomic and cluster ions sputtered from the target to an angle of 90° were extracted through a 1-mm-diam aperture positioned 7 mm apart from the target. They were then accelerated and focused with an einzel lens onto a 6-mm-diam entrance slit of a magnetic mass analyzer. The analyzed secondary ions which passed through a $(1\times5)$-$mm^2$ slit were detected with a channel electron multiplier (Ceratron) [19]. The vacuum chamber was baked beforehand at approximately 120 °C for 2 days. The pressures of $10^{-7}$ Pa and $10^{-6}$ Pa were achieved for the isolated and the experimental conditions, respectively. The front surface of each target was purified by bombarding intense Si ions for 1 h before taking mass spectra.

The mass spectra of the secondary positive and negative ions were taken by sweeping magnetic field by a step of 0.001 T from 0 to 0.5 T corresponding to the mass range up to 130 u/$e$. The mass resolution of 1.6% was obtained. The field step was small enough to observe mass peak profile. Measurements of mass spectra were carried out at several incident energies between 0.4 and 10 MeV at a fixed particle flux of $1.3\times10^{12}$ $s^{-1}\,cm^{-2}$ for $Si^{q+}(q = 1,2,3,4,5,6)$ and for $C^{q+}$, $Ge^{q+}$, and $Ag^{q+}(q = 1,2,3,4)$ projectiles. The beam intensities were monitored before and after each run. Counting rates were kept below about $5\times10^5$ $s^{-1}$, which was tolerable for the Ceratron multiplier. In the case of the $SiO_2$ target, the ranges of the incident ions were longer than the thickness of the $SiO_2$ layer. Then the incident ions passed through the layer and stopped in the electrically conductive Si wafer. This successfully prevented the target from the electrical charging up. On the other hand, the layer was thick enough to withstand the bombardment for about $3\times10^5$ s before being sputtered out. The obtained mass spectra were reproducible and hardly depended on the charges of incident elemental species.

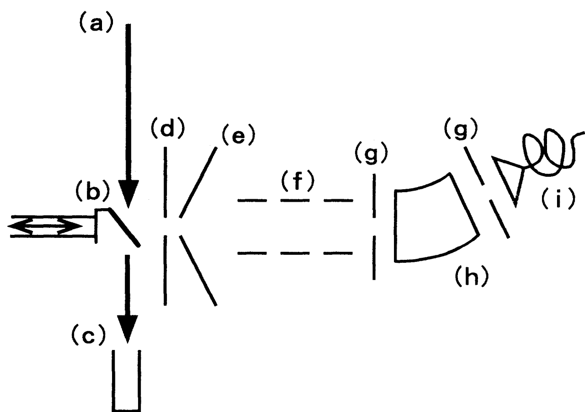


FIG. 2. Schematic diagram of the experimental arrangement for secondary-ion detection: (a) primary ion beam, (b) target, (c) Faraday cup, (d) aperture, (e) accelerating electrode, (f) einzel lens, (g) collimators, (h) selecting magnet, and (i) electron multiplier.

## III. RESULTS

Examples of the mass spectra of secondary-ion species are shown in Figs. 3(a) and 3(b) for the Si and $SiO_2$ targets bombarded by $Si^{3+}$ projectiles, respectively. As known from Fig. 3(a), the most dominant species was $Si^+$ and multiple-charged atomic-silicon species were observed too. Weak background peaks originating from adsorbates on the surface of the target were attributed to $H^+$, $O^+$, $H_3O^+$, $Na^+$, and $K^+$. For the case of the $SiO_2$ target, other than the ions mentioned above, some molecular and cluster ions were observed.

The secondary-ion yields from the Si target are plotted in Figs. 4(a)–4(d) as a function of incident energy for the C, Si, Ge, and Ag projectiles, respectively. The yields for the $SiO_2$ target are shown in Figs. 4(e)–4(h) for the respective four incident species. Those values of $Si^-$ and $O^-$ ions from the $SiO_2$ target are also presented in Fig. 5 for the Si and Ag projectiles. The individual values in Figs. 4 and 5 are the means of at least three

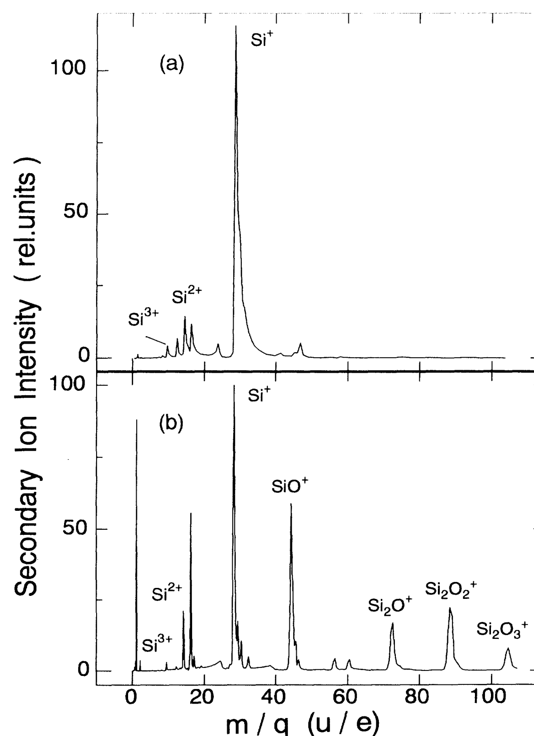


FIG. 3. Examples of mass spectra of secondary ions for the (a) Si and (b) $SiO_2$ targets.

determinations. The experimental errors result primarily from variability of the secondary-ion emission caused by the surface condition of the target and from the uncertainty in the overall efficiency of the mass analyzer. The standard deviations of the respective measurements are at most 7%. Statistical errors were in all cases insignificant.

Figures 4(a) and 4(e) show that the yields for the C projectiles are generally decreasing functions of incident energy. In addition, the energy dependence of the yields of lightly charged secondary ions is stronger than that for multiple-charged ions. On the contrary, as shown in Figs. 4(d) and 4(h), for the Ag projectiles the yields increase with increasing incident energy except for the $Si^+$ ions. The yield curves for the Si and Ge projectiles are rather similar to those for the C and Ag ions, respectively. Figure 5 shows that the behaviors of the $O^-$ and $Si^-$ ions resemble those of the $Si^+$ ions.

Figures 6(a)–6(h) show the yield ratios of the $Si^{q+}$ ($q = 2, 3, 4$) ions relative to the $Si^+$ ions plotted vs the incident energy. The ratios increase rapidly at first, and then level off or decrease with incident energy for all the projectiles. Most of the yield ratios of multiple-charged ions are higher for the light incident species than for heavy species. This fact suggests a dependence on the amount of electronic energy deposited, since the electronic energy depositions are prominent in C projectiles, but in Ag the nuclear contribution still works in the present energy range. The yields of $Si^+$ and the multiple-charged secondary Si ions are probably sensitive to the nuclear and electronic energy depositions, respectively. This feature is displayed in the yield curves of $Si^{4+}$, whose yields increase more rapidly with increasing incident energy than those of $Si^{2+}$ and $Si^{3+}$.

## IV. DISCUSSION

So far, the mechanisms based on the nuclear energy deposition have been widely accepted in the explanation of

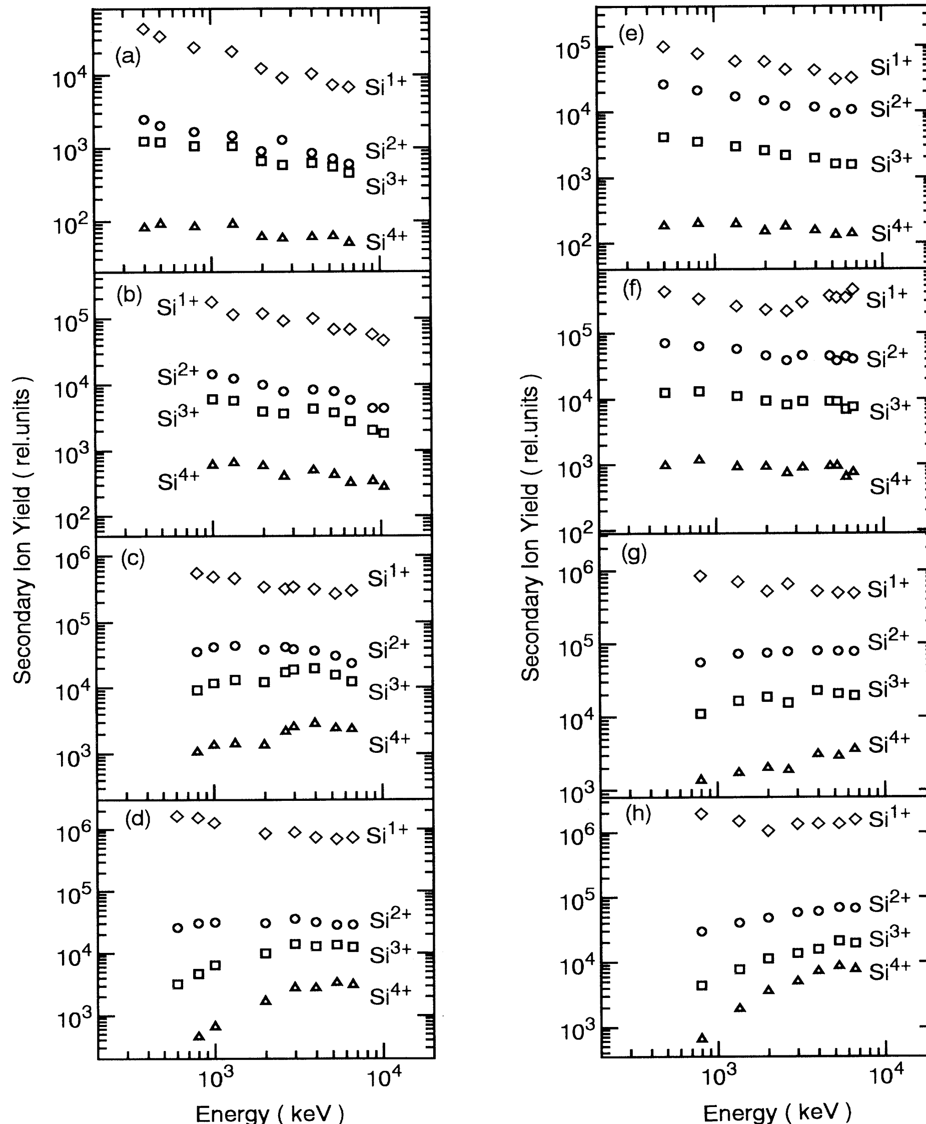


FIG. 4. Incident-energy dependence of the multiple-charged positive secondary-ion yield for the Si and $SiO_2$ targets bombarded by the C, Si, Ge, and Ag projectiles: (a) C+Si, (b) Si+Si, (c) Ge+Si, (d) Ag+Si, (e) C+$SiO_2$, (f) Si+$SiO_2$, (g) Ge+$SiO_2$, and (h) Ag+$SiO_2$. The experimental errors are at most 7% and are comparable to or smaller than the sizes of the respective marks.

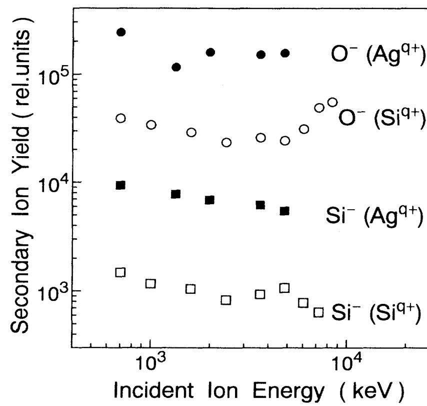


FIG. 5. Incident-energy dependence of the negatively charged secondary-ion yield for the $SiO_2$ target bombarded by the Si and Ag projectiles. The experimental errors are at most 7% and are comparable to or smaller than the sizes of the respective marks.

the secondary-ion emission under low-energy bombardment. Therefore, in Figs. 7(a) and 7(b), the yields of $Si^+$ and $Si^{4+}$ ions are plotted as a function of $S_n$ for the Si and $SiO_2$ targets. In the $Si^+$-Si case, the experimental data are well fitted with a curve of $S_n^{0.78}$ and the fact implies that the $Si^+$ ions are produced through the nuclear-collision mechanism still in the high-energy range under consideration. The yields of the $Si^+$ ions from the $SiO_2$ target are larger than the corresponding yields from the Si target and the result agrees with the general prediction in the framework of the bond-breaking concept [3,4].

However, in the case of $Si^{4+}$, as shown in Fig. 7(b), the yields have little correlation to $S_n$. This finding requires other mechanisms of secondary-ion emission not addressed by the current models of secondary-ion emission. Blauner and Weller measured the secondary Al-ion yields from aluminum and aluminum oxide bombarded by rare-gas ions at energies below 275 keV and reported

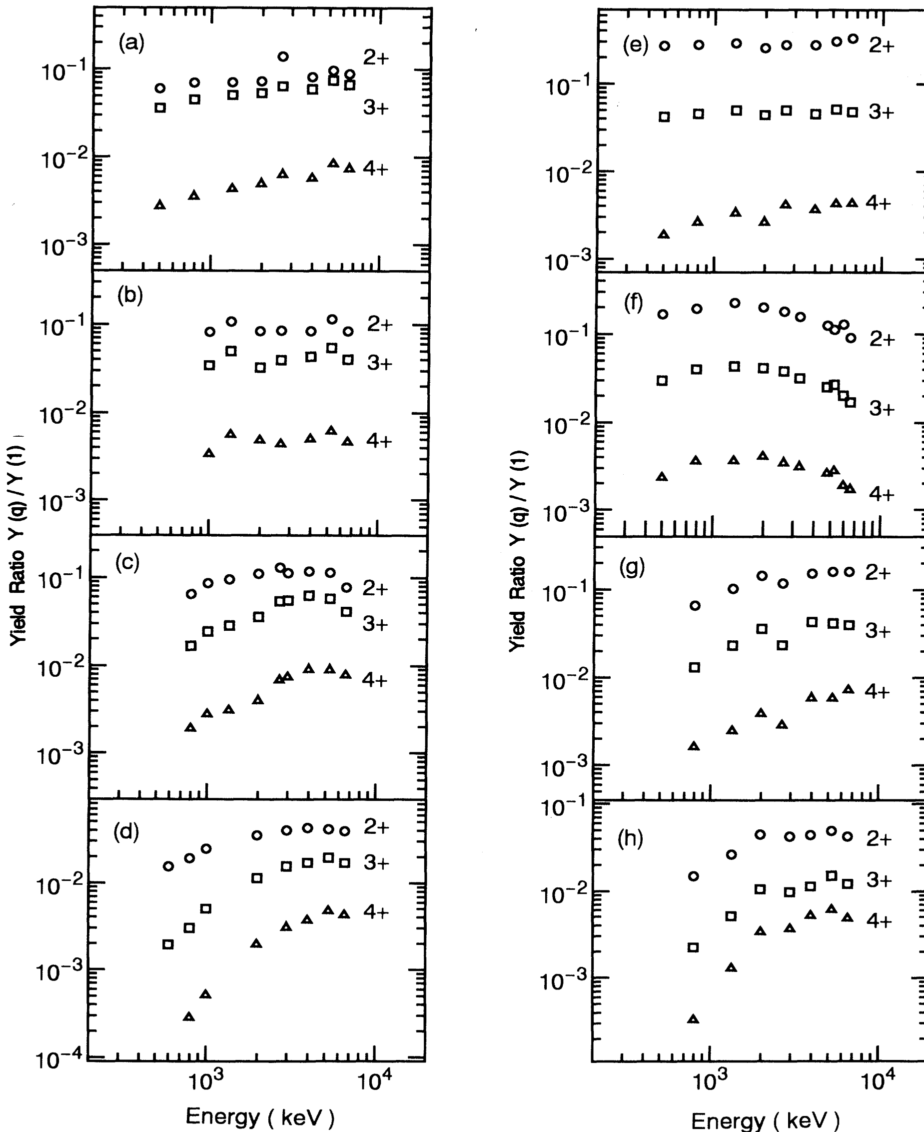


FIG. 6. Yield ratios of $Si^{q+}$ ions ($q = 2,3,4$) relative to $Si^+$ ions are plotted as a function of incident energy for the Si and $SiO_2$ targets bombarded by the C, Si, Ge, and Ag projectiles: (a) C+Si, (b) Si+Si, (c) Ge+Si, (d) Ag+Si, (e) C+$SiO_2$, (f) Si+$SiO_2$, (g) Ge+$SiO_2$, and (h) Ag+$SiO_2$. The circles, squares, and triangles represent the charge states of the secondary ions of 2+, 3+, and 4+, respectively.

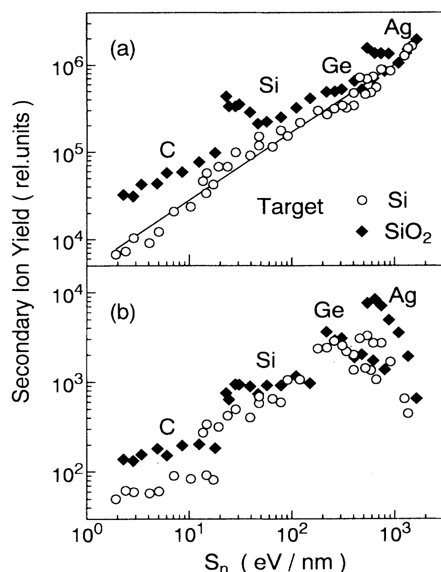


FIG. 7. Yields of secondary $Si^+$ and $Si^{4+}$ ions are plotted as a function of the nuclear stopping power: (a) $Si^+$ and (b) $Si^{4+}$. The experimental data of $Si^+$ from the Si target are well fitted with a curve of $S_n^{0.78}$ shown with the solid line.

that multiple-charged ions are produced by the kinetic mechanism [11,15]. In this mechanism, the intensities of secondary ions vary similarly to $S_n$. In the same experiment, however, they found that $O^+$ ions emitted from the oxide surface are produced by means of a mechanism wholly unrelated to $S_n$. Its production cannot be explained by any of the proposed models of metallic secondary-ion emission. As described above, the yields of the $Si^{4+}$ ions shown in Fig. 7(b) meet the same situation at high incident energies. In order to explain their production rates, one needs other parameters in addition to $S_n$. A promising mechanism in the high-energy region should contain any direct ionization caused by the collisions of projectiles with target atoms. For the moment it is assumed that, in ionization of Si atoms up to a charge $q = 4$, four electrons in the $M$ shell play a main role, while the $L$-shell and $K$-shell electrons play a minor role,

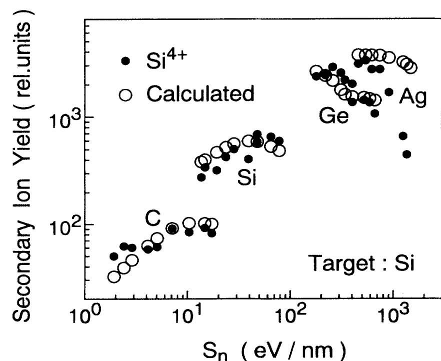


FIG. 8. Secondary yields of $Si^{4+}$ ions are compared with a multiple of the nuclear $S_n$ and electronic $S_e$ stopping powers. The solid circles denote the experimental results and the open circles denote the calculated values of $S_n^{0.78}S_e$.

and the ionization probability is proportional to the electronic stopping power $S_e$. Figure 8 shows the comparison between the experimental data of the secondary $Si^{4+}$ ions from the Si target and the calculated values [16] of $S_n^{0.78}$ multiplied by $S_e$. Here the function $S_n^{0.78}$ is arbitrarily used to take account of the recoil process, because the function explains well the $Si^+$-ion yield. The calculation reproduces rather well the experimental results, except for the Ag projectiles. This indicates the importance of the direct ionization by the primary ions. That is, the simultaneous process of ionization and recoil caused by the projectiles probably produces the multiple-charged ions.

It is known in fact that multiple-charged recoil ions are produced effectively in collision between energetic highly charged ions and, for example, rare-gas targets [20–22]. Although no complete understanding of multiple ionization of atoms by energetic heavy-ion impact is possible at present, some reasonable description of such a process can be made in the framework of the independent-electron model [20–22]. The model is applied in the incident-energy region several times higher than the orbital velocities of the electrons being removed and predicts that the multiple-charged ions are produced through not only a pure-ionization process, but transfer ionization in which the projectile captures electrons from the target atom.

In the present experiment, the multiple-charged secondary ions were produced from the solid targets and their yields correlate with the multiples of two factors [18] of $S_n$ and $S_e$ as described above. It is then plausible that the atoms on the surface are simultaneously ionized and recoiled by the same projectiles. Thus it is worth comparing the experimental results for the solid targets with those for the gas targets and with the prediction by the independent-electron model [20–22].

According to the independent-electron model [20–22], the cross sections for multiple ionization of recoiled atoms are given by the sum of cross sections for pure ionization and ionization accompanying the electron-loss and -capture processes and are expressed as

$$\sigma(q,q';i) = \int \begin{bmatrix} n \\ i \end{bmatrix} P_V^i (1-P_V)^{n-i} 2\pi b \, db, \qquad (1)$$

where $q$ and $q'$ are the charges of projectiles before and after the collision, respectively, $i$ is the charge of the recoiled ions, $n$ is the number of electrons in the outer shell, $P_V$ is the ionization probability of one of the outer-shell electrons, and $b$ is the impact parameter of collisions. For

TABLE I. Used parameters $P_V$ and $r_V$ (in nm) for electron-loss and -capture ionization processes ($q \neq q'$) and $P_V(0)$ and $r_V$ (in nm) for pure ionization ($q = q'$).

| $q$ | $q'$ | $P_V$ | $r_V$ |
|---|---|---|---|
| 2 | 2 | 0.019 | 0.049 |
| 2 | 3 | 0.028 | 0.036 |
| 4 | 3 | 0.034 | 0.007 |

| $q$ | $q'$ | $P_V(0)$ | $r_V$ |
|---|---|---|---|
| 2 | 2 | 0.035 | 0.033 |
| 4 | 4 | 0.040 | 0.055 |

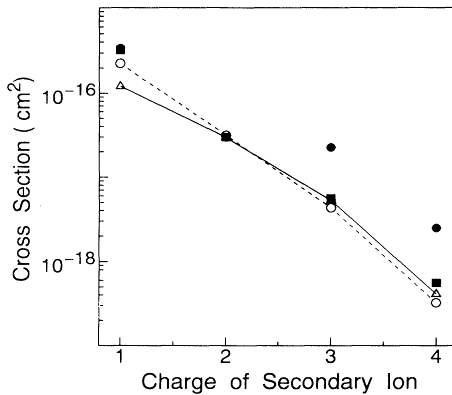


FIG. 9. Yield dependence on the charges of secondary ions is compared with the prediction based on the independent-electron model. The used parameters are given in Table I. The solid line with triangles and the dotted line with open circles represent the calculated results for the incident 2+ and 4+ ions, respectively. The closed circles and closed rectangles are experimental results at an energy of 6.6 MeV for the C+Si and Si+Si systems, respectively, and are normalized arbitrarily at the charge of 2+.

ionization accompanying the electron-loss and -capture processes $P_V$ is assumed to be constant inside an impact parameter $r_V$ and zero outside [22]. Then the cross sections for those processes are expressed as

$$\sigma(q,q';i) = \begin{bmatrix} n \\ i \end{bmatrix} P_V^i (1-P_V)^{n-i} r_V^2 \pi. \qquad (2)$$

On the other hand, for pure ionization it is better to assume that the parameter $P_V$ depends on the impact parameter exponentially [22],

$$P_V(b) = P_V(0)\exp(-b/r_V), \qquad (3)$$

where $P_V(0)$ represents the ionization probabilities of the outer-shell electrons at the impact parameter $b = 0$. Systematic experimental studies of the independent-electron model are very few and it is difficult to fix the parameters for our processes. As a first approach, we take the values [22] for a $Ne^{q+}$ + Ne system at an energy of 1.05 MeV/u, as given in Table I for incident charges of 2 and 4, but change the number of the outer-shell electrons from 8 in the Ne system to 4 for the present Si recoils.

The calculated results are plotted in Fig. 9 along with the experimental data for the C-Si and Si-Si systems. It is difficult to compare the calculated values quantitatively with the experimental results by lack of reliable parameters applied to the present collision systems. In addition, it is possible for multiple-charged ions to change their charges after the collisions on their passages through a few atomic layers and on leaving the solid surface. However, the qualitative agreement between them implies that the multiple-charged recoil ions are probably produced through the simultaneous process of ionization and recoil caused by the projectiles. For further confirmation it is necessary to measure the production cross sections of the multiple-charged recoil ions for systematic incident and recoiled species in a wide energy range of the projectiles. It is also necessary to take into account more rigidly the Auger ionization and charge-exchange processes: the former for the excited recoils to suffer on leaving from the surface and the latter inside the solid and in the atmosphere of sputtered atoms and clusters [23].

## V. CONCLUSIONS

The secondary-ion yields have been measured for the Si and $SiO_2$ targets bombarded by the C, Si, Ge, and Ag projectiles over the wide energy range up to 10 MeV, where the electronic collision becomes more prominent than the nuclear collision in energy deposition even for the Ag projectiles. The $Si^{q+}$ species with charges $q$ up to 4+ were clearly observed for all the collision systems. The yields for the C projectiles are generally decreasing functions of incident energy irrespective of the charge of the secondary ions. On the other hand, for the Ag projectiles they increase with increasing energy except for $Si^+$. In addition, the yield ratios of $Si^{q+}$ ($q = 2,3,4$) relative to $Si^+$ are higher for the light incident species than for heavy species, and the yields of $Si^{4+}$ increase with increasing energy more rapidly than those of $Si^{2+}$ and $Si^{3+}$ for the heavy incident species. These facts reflect a large contribution of electronic energy depositions in the formation of the multiple-charged ions. Indeed, the experimental yields of the secondary $Si^{4+}$ ions from the Si target are well reproduced by the calculated values of $S_n^{0.78}$ multiplied by $S_e$. The qualitative reproduction is obtained moreover for the yield dependence on the charges of secondary ions based on the independent-electron model, which describes multiple ionization of atoms by energetic heavy-ion impact. From these facts we could conclude that the multiple-charged recoil ions are produced through the simultaneous process of ionization and recoil caused by the projectiles in the dominant region of the electronic collision.

## ACKNOWLEDGMENTS

This work was done with the Experimental System for Ion Beam Analysis at Kyoto University. We thank K. Yoshida, K. Norisawa, and Dr. T. Ohdaira for their useful advice and technical support during the experiments. It has been supported in part by a Grant-in-Aid for Scientific Research from the Ministry of Education, Science, and Culture of Japan.

[1] For recent review see Ming L. Yu, in *Sputtering by Particle Bombardment III,* edited by R. Behrisch and K. Wittmaack (Springer, Berlin, 1991), p. 91.
[2] W. F. van der Weg and P. K. Rol, Nucl. Instrum. Methods **38**, 274 (1965).
[3] M. L. Yu and N. D. Lang, Phys. Rev. Lett. **50**, 127 (1983).
[4] G. Slodzian, Surf. Sci. **48**, 161 (1975).
[5] M. L. Yu and K. Mann, Phys. Rev. Lett. **57**, 1476 (1986).
[6] P. Williams, Phys. Rev. B **23**, 6187 (1981).
[7] O. Becker, W. Knippelberg, and K. Wien, Phys. Scr. **T6**, 117 (1983).
[8] J. P. O'Connor, P. G. Blauner, and R. A. Weller, Nucl. Instrum. Methods B **13**, 338 (1986).
[9] J. F. Hennequin, J. Phys. (Paris) **29**, 655 (1968).
[10] K. Wittmaack, Nucl. Instrum. Methods **170**, 565 (1980).
[11] P. G. Blauner and R. A. Weller, Phys. Rev. B **35**, 1492 (1987).
[12] P. Joyes, Radiat. Eff. **19**, 235 (1973).
[13] U. Fano and W. Lichten, Phys. Rev. Lett. **14**, 627 (1965).
[14] J. J. Vrakking and A. Kroes, Surf. Sci. **84**, 153 (1979).
[15] P. G. Blauner and R. A. Weller, Phys. Rev. B **35**, 1485 (1987).
[16] B.U.R. Sundqvist, in *Sputtering by Particle Bombardment III,* (Ref. [1]), p. 256 and references cited therein.
[17] D. Fenyö, B. U. R. Sundqvist, and B. R. Karlsson, Phys. Rev. B **42**, 1895 (1990).
[18] J. F. Ziegler, *Handbook of Stopping Cross Section for Energetic Ions in All Elements* (Pergamon, New York, 1980); J. P. Biersack and J. F. Ziegler, TRIM code.
[19] Murata Mgf. Co., Ltd., Japan.
[20] R. E. Olson, J. Phys. B **12**, 1843 (1979).
[21] J. Ullrich, K. Bethge, S. Kelbch, W. Schadt, H. Schmidt-Böking, and K. E. Stiebing, J. Phys. B **19**, 437 (1986).
[22] H. Tawara, T. Tonuma, H. Kumagai, and T. Matsuo, Phys. Rev. A **41**, 116 (1990).
[23] J. W. Rabalais and J. N. Chen, J. Chem. Phys. **85**, 3615 (1986).